Toward transduodenal diffuse optical tomography of proximal pancreas

Daqing Piao,[1,*] Kenneth E. Bartels,[2] Russell G. Postier,[3] G. Reed Holyoak,[2] and Jerry W. Ritchey[4]

[1]*School of Electrical and Computer Engineering, Oklahoma State University, Stillwater, Oklahoma 74078, USA*

[2]*Department of Veterinary Clinical Sciences, Oklahoma State University, Stillwater, Oklahoma 74078, USA*

[3]*Department of Surgery, University of Oklahoma Health Sciences Center, Oklahoma City, Oklahoma 73126, USA*

[4]*Department of Veterinary Pathobiology, Oklahoma State University, Stillwater, Oklahoma 74078, USA*

**Corresponding author: daqing.piao@okstate.edu*

Received June 26, 2013; revised September 8, 2013; accepted September 11, 2013;
posted September 16, 2013 (Doc. ID 192872); published October 10, 2013

We demonstrate the feasibility of diffuse optical tomography (DOT) of the proximal pancreas by using optical applicator channels deployed longitudinally along the exterior surface of a duodenoscope. As the duodenum that nearly encircles the proximal pancreas forms a natural "C-loop" that is approximately three-quarters of a circle of 5–6 cm in diameter, a multichannel optical applicator attached to a duodenoscope has the potential to perform transduodenal DOT sampling of the bulk proximal pancreas wherein most cancers and many cystic lesions occur. The feasibility of transduodenal DOT is demonstrated on normal porcine pancreas tissues containing an introduced gelatinous inclusion of approximately 3 cm in diameter, by using nine source channels and six detector channels attached to a duodenoscope. Concurrent ultrasonography of the gelatinous inclusion in the porcine pancreas parenchyma provided a coarse, albeit indispensable, anatomic prior to transduodenal DOT in reconstructing a contrast of optical properties in the pancreas.

OCIS codes: (170.6960) Tomography; (170.2680) Gastrointestinal; (170.2150) Endoscopic imaging; (170.3880) Medical and biological imaging.

http://dx.doi.org/10.1364/OL.38.004142

The pancreas is difficult to access nondestructively by diagnostic methods due to its challenging anatomic location. Partially because of this difficult accessibility, malignancies of the pancreas are often discovered at a late, nonresectable stage, leaving the patients and physicians with very limited options of effective clinical management [1]. The overall prognosis of malignancy of the pancreas is poor, currently estimated to have an approximately 75% mortality rate in the first year of diagnosis and a five-year survival rate of only 6% [2] after decades of efforts to find better treatment strategies [3]. One type of pathological condition of the pancreas requiring careful risk stratification is intraductal papillary mucinous neoplasm (IPMN), a cystic lesion with a thick gelatinous interior that forms in major pancreatic duct or accessory duct or is mixed [4]. It is established that the primary-duct-type IPMN has high risk to become malignant and thus is recommended for resection [5]. However, resection of the branch duct type IPMN has been controversial [6] due to lack of consensus on the malignant potential [7] as well as lack of specific radiological or surrogate imaging markers for risk stratification of it [8].

Optical approaches have been explored for early detection of pancreatic cancer and differentiating between cancerous and noncancerous such as inflammatory pancreatic tissues that often have nonspecific symptoms. Chandra *et al.* [9] reported highly specific reflectance spectroscopy and fluorescence measurement of specimens of pancreatectomy and xenografts of pancreatic carcinoma in nude mice by *in situ* probing using an optical applicator consisting of three closely positioned fibers. Liu *et al.* [10] studied the light scattering markers of the duodenal mucosal layer that indicated or predicted early stage malignant development in the pancreas. Iftimia *et al.* [11] demonstrated that optical coherence tomography (OCT) imaging discriminates the morphological features of pancreatic cystic lesions of different risk potentials.

Among the lesions of the pancreas that are malignant or have malignant potential, the majority are discovered in the head of pancreas [12], and a cystic lesion of at least 2 cm in size is not uncommon [13]. To aid in the decision making for surgical intervention and potential resection of a particular lesion, a preoperative imaging evaluation of the lesion is essential. The optical fingerprints potentially expressed in the duodenal mucosal layer [10] could prospectively predict the existence of, albeit do not directly "image," a lesion in the pancreas. An optical applicator that probes tissue using reflectance geometry [9] is limited in nondestructively interrogating a large nonsuperficial lesion. Intraductal OCT probing [11], which reveals high-resolution morphological features over a 2 mm depth, of a cystic lesion of significant size may involve multiple needle-invasive procedures. An optical method to nondestructively image the bulk pancreas is of considerable interest.

This Letter demonstrates the feasibility of transduodenally imaging the proximal pancreas by a diffuse optical tomography (DOT) method. As conceptualized in Fig. 1(a), the proximal pancreas is nearly encircled by the duodenum in a "C-loop" geometry that approximates three-quarters of a circle. As pancreatic tissue is scattering-dominant at wavelengths greater than 600 nm [14], it may be feasible to perform DOT sampling of the proximal pancreas, which has a cross-sectional dimension of 5–6 cm in diameter and a thickness of less than 2 cm, through the duodenum by deploying multiple channels of optodes along a duodenoscope.

Figure 1(b) shows a prototype optical-applicator with 15 optical fibers deployed along the exterior surface of a duodenoscope. Figure 1(c) depicts the designed

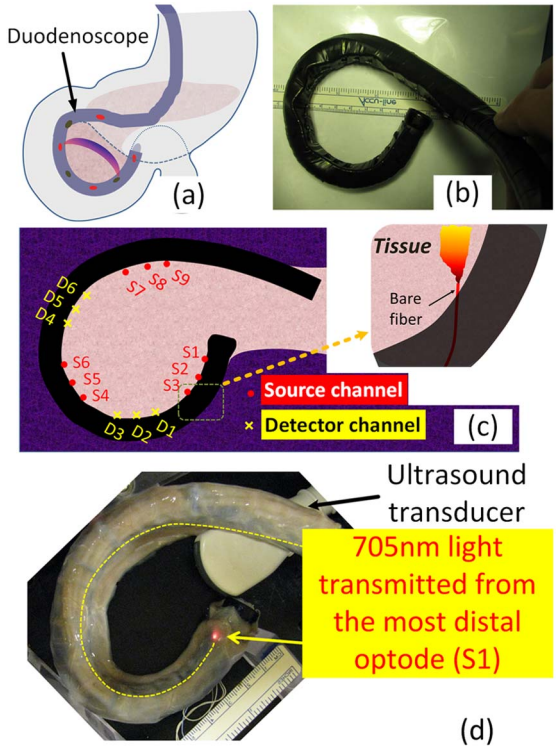

Fig. 1. (a) Natural "C-loop" of duodenum renders the possibility to optically sample the entire proximal pancreas. (b) A total of 15 fibers (nine for source and six for detector) have been attached onto a duodenoscope. (c) Designed positions of the 15 fibers along the duodenoscope. The inset illustrates that the bare fiber as the optode is obliquely positioned with respect to the duodenoscope and that the optode has an inward- and forward-looking geometry for source illumination and detector collection. (d) The duodenoscope-attached optical applicator is passed through a porcine duodenum; a red guiding light transmitted through the duodenum from the most distal source is visible as shown by the arrow.

locations of the nine source optodes (marked by circle, 400 μm core diameter) and six detector optodes (marked by cross, 600 μm core diameter) that are longitudinally positioned on the duodenoscope. The nine source channels (S1 to S9) are separated to three groups, each consisting of three adjacent channels. The six detector channels (D1 to D6) are separated to two groups, each also consisting of three adjacent channels. The two detector groups separate the three source groups. Compared to uniformly interspersing each source with each detector, the shown positioning of the source or detector channels increases the minimum source-detector distance while the maximum source-detector distance is set by the dimension of the geometry. This optode configuration reduces the total dynamic range of the signals and better accommodates the measurement by a single CCD detector. The targeted arc distance between adjacent channels in each source or detector group was 10 mm, and the targeted arc separation between the neighboring source and detector groups was 20 mm. After forming the duodenoscope to the "C" shape, however, the positions of the optodes shifted and were measured individually. The proximal ends of all of these fibers were terminated with sub-miniature version A (SMA) 905 connectors. Figure 1(d) is the photograph of a porcine duodenum, through which the duodenoscope-attached optical applicator was inserted, and the most distal source channel (S1) was made visible by the transmitted 705 nm guiding light. Also photographed in Fig. 1(d) is a convex ultrasound (US) transducer, which was placed as a concurrent anatomic reference to the DOT measurement of tissue. The measurement configuration involving US imaging as shown in Fig. 1(d) could become more relevant to transduodenal imaging of the pancreas should an endoscopic US transducer probe passing through the instrument channel of the duodenoscope be used.

This study performed continuous-wave (CW) DOT measurement at 705 nm, at which wavelength the reduced scattering coefficient of normal pancreatic tissue was shown close to 1.4 mm^{-1} [14]. The schematic of the DOT measurement system is given in the upper panel of Fig. 2, and the lower panel of Fig. 2 includes photographs of the fiber channels branched from the duodenoscope and the measurement system placed in the Biomedical Surgical Laser Laboratory in the Center of Veterinary Health Sciences of Oklahoma State University. The 705 nm light from a thermally stabilized laser diode was coupled through a 200 μm fiber to a 1×9 fiber switch (Piezosystem) for sequential delivery to the nine source channels of the duodenoscope-attached optical applicator. The six detector fibers were coupled to a spectrometer (Princeton Instruments Spectropro2300i) to which an intensified CCD camera (Acton Research PI-MAX Gen-II) was mounted. The acquisition time corresponding to each source channel took between 250 ms and 1 s, depending upon the gain setting of the CCD. An ALOKA Proscan 7 console and a convex transducer (UST-9120) were used for concurrent ultrasonography. The DOT image reconstruction was rendered by NIRFAST [15,16].

Given only 54 measurements at CW and at a single wavelength, this DOT system is limited in the capacity to recover tissue optical heterogeneities. Therefore this

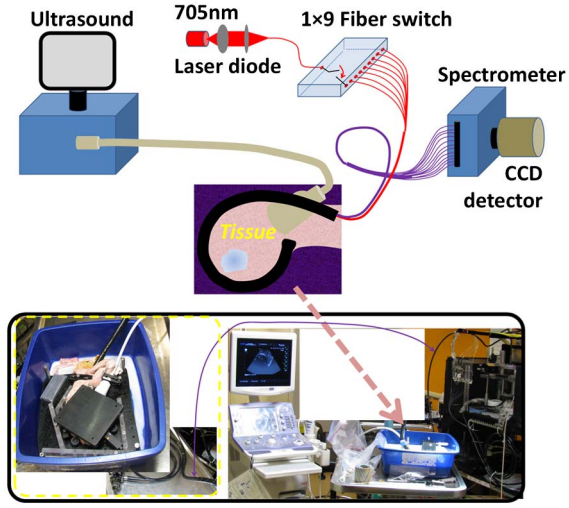

Fig. 2. Top panel shows the schematic of the system for US-coupled transduodenal DOT. The dashed arrow points to the tissue/applicator setup contained in a blue receptacle, of which the photograph is shown in the left. The fiber bundle branched from the duodenoscope for optical tomography measurement is also marked by the solid line pointing to two photographs.

DOT work only considered the absorption contrast that could have been contaminated by the scattering contrast in the reconstruction. The demonstration was further impaired by the difficulty to accurately profile the imaging geometry because the distal end of the duodenoscope could not be articulated to a perfect circle and after forming to the C-shape the medium-facing concave surface of the duodenoscope became irregular, which further distorted the positioning of the obliquely attached optodes. For the purpose of calibration, the duodenoscope-attached optical applicator was placed in a cylindrical retainer made from black acetal materials, as illustrated in Fig. 3(a). The measured optode positions, the radial and azimuthal coordinates shown in Fig. 3(b) and the height variations marked in Fig. 3(c), are set in an approximate imaging volume of a cylinder of 55 mm in diameter and 18 mm in thickness corresponding to the volume of the intralipid framed by the duodenoscope. An example of the signals corresponding to the 54 source-detector pairs measured from, or calculated for, the homogenous medium is shown in Fig. 3(d). The medium used for calibration purpose was a 0.5% bulk intralipid solution with an absorption coefficient of 0.003 mm^{-1} and reduced scattering coefficient of 0.50 mm^{-1}.

An inclusion of 16 mm in cross-section was positioned at four quadrangles of the imaging geometry to test the system performance in reconstructing an object of absorption contrast at different azimuthal locations. The locations correspond to 4:30, 7:30, 10:30, and 1:30 o'clock positions as marked by the dashed circles in Fig. 3(e) and 3(f). The 1:30 o'clock position, since it is located near the opening of the "C-loop", was expected to be the least accurately reconstructed among the four positions. The DOT reconstruction incorporated the spatial information, namely the size and position, of the object, assuming absorption contrast only. When a black object was used as the inclusion, the inclusion was clearly reconstructed, as shown in Fig. 3(e), with the peak absorption coefficients at 0.054, 0.051, 0.045, and 0.072 mm^{-1} respectively for the four locations. When an object of known absorption coefficient of 0.0061 mm^{-1} was used, the object was clearly identified at only one location and poorly recovered at three other locations, as shown in Fig. 3(f), and the peak absorption coefficients were 0.0029, 0.0028, 0.0086, and 0.0031 mm^{-1} respectively for the four locations. It is worth noting that, without implementing the size and position of the object to the DOT image reconstruction, the inclusion was unremarkable even when the black object was imaged.

To mimic transduodenal DOT of the pancreas tissue under endoscopic or transabdominal US guidance, the optical applicator-attached duodenoscope that was inserted into a segment of duodenum and the convex US transducer were formed into C-shape associated positions, as photographed in Fig. 1(d), on a black acetal platform by using multiple pieces of isolated retainers. The entire black platform was then immerged in a 0.91% bulk intralipid solution to produce an effective transduodenal imaging volume of 2 cm in thickness. The absorption coefficient and reduced scattering coefficient of the medium were 0.003 and 0.91 mm^{-1}, respectively. Two specimens of normal porcine pancreas were stacked to approximately 2 cm in thickness to fill the

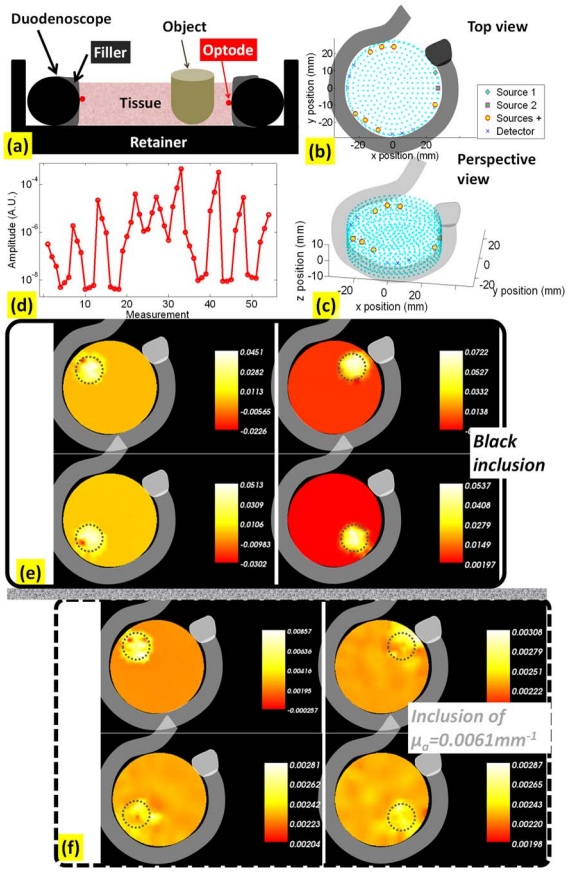

Fig. 3. (a) Applicator configuration for testing the performance of the system in reconstructing an object of absorption contrast at different azimuthal locations. The medium-facing side of the duodenoscope was modified to nearly flat by using black filling materials to make the geometry closer to a cylinder. The interfacing of the medium with the air at the top surface, however, was unaltered. (b) The top view of the mesh shows the measured optode locations. Circles: sources; crosses: detectors. Slight variation of the radial positions of the optodes can be observed. (c) The perspective view of the mesh shows the notable variation of the elevational positions of the optodes. (d) Example pattern of CW amplitudes (natural log scale) corresponding to 54 source-detector pairs measured from a homogenous medium. (e) DOT of a 16 mm black inclusion placed in the four quadrangles of the imaging geometry. The reconstruction incorporated the spatial prior information including the position and size of the object. (f) DOT of a 16 mm phantom inclusion of known absorption coefficient of 0.0061 mm^{-1} placed at the same positions as the black object of (e). The reconstruction incorporated the spatial prior information including the position and size of the object.

space between the duodenoscope and the US transducer. A segment of porcine duodenum of approximately 3 cm in diameter containing thick aqueous solution of porcine gelatin (Sigma Life Science, St. Louis, Missouri) was placed between the porcine pancreas and the duodenoscope, as shown by the photograph at the top panel of Fig. 4. The arrow at the leftmost US image at the middle panel of Fig. 4 marks the gelatinous solution housed by the duodenum. The middle US image in Fig. 4 corresponds to replacing the gelatinous inclusion with a piece of porcine liver (arbitrary shape), and the rightmost US image indicates a void space produced in the pancreas tissue and filled by the background intralipid solution.

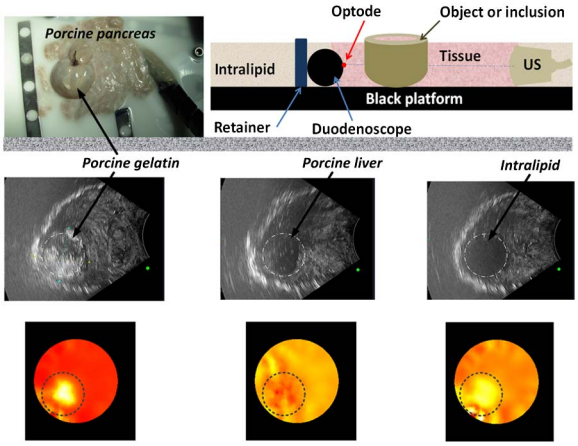

Fig. 4. Top panel: A segment of porcine duodenum containing thick gelatinous solution was placed in the stacked porcine pancreas. The duodenoscope was inserted in a duodenum, part of which can be seen in the photograph at the left, for transduodenal DOT of the stacked porcine pancreas in the intralipid solution. The schematic at the right side shows the side view of the imaging configuration. Middle panel: Ultrasonography shows the inclusion made from porcine gelatin (left), the inclusion of porcine liver (middle), and the inclusion of intralipid filling a void-space of the pancreas (right). Bottom panel: Reconstructed transduodenal DOT images corresponding to the inclusions shown at the middle panel. The reconstruction assumed an absorption object of 3 cm in diameter at the shown 7:30 o'clock position.

The irregular shape of the optical applicator-attached duodenoscope is observable from the US image. The volume of the tissue to be imaged is, for convenience, represented by a cylinder of 56 cm in diameter and 2 cm in thickness. The inclusions shown in US were estimated to have a 3 cm diameter. The bottom-panel presents the three inclusions reconstructed by incorporating the inaccurate, but indispensable, size and location of the inclusion in the tranduodenal DOT. A remarkable and relatively homogenous contrast was reconstructed in the delineated region corresponding to an inclusion made of either the duodenum-enclosed gelatinous material or the intralipid-filled tissue-voided inclusion. However, the inclusion corresponding to porcine liver tissue of unrestricted shape was poorly differentiable.

In summary, DOT imaging of the proximal pancreas seems feasible. Pancreatic tissue is highly scattering, and the proximal pancreas has a cross-sectional dimension of 5–6 cm in diameter, a size suitable for DOT sampling. As the proximal pancreas is encircled over approximately three-quarters of the peripheral by the duodenum "C-loop," optical applicator channels attached to a duodenoscope can perform transduodenal DOT sampling of the bulk proximal pancreas. This feasibility is demonstrated on normal porcine pancreas tissues containing a gelatinous inclusion by CW DOT at a single wavelength, with coarse spatial information of the inclusion provided by US. It is expected that DOT, utilizing spectroscopy measurement, time- or frequency-domain detection, and accurate anatomic information available from imaging modalities such as high-volume computed tomography and fiducial markers, has the potential to provide radiological optical contrast of the lesions in proximal pancreas.

The authors acknowledge the Oklahoma Animal Disease Diagnostic Laboratory and Oklahoma Food and Animal Product Resources Center for acquisition of porcine tissues. Piao thanks graduate students Nigar Sultana and Krishna Tokala for technical assistance. This research is made possible in part by a health research grant HR11-043 from the Oklahoma Center for the Advancement of Science and Technology (OCAST) and an endowment (to Bartels) from the Kerr Foundation.

References

1. I. T. Konstantinidis, A. L. Warshaw, J. N. Allen, L. S. Blaszkowsky, C. F. Castillo, V. Deshpande, T. S. Hong, E. L. Kwak, G. Y. Lauwers, D. P. Ryan, J. A. Wargo, K. D. Lillemoe, and C. R. Ferrone, Ann. Surg. **257**, 731 (2013).
2. American Cancer Society, *Cancer Facts & Figures 2013* (American Cancer Society, 2013).
3. M. W. Saif, N. A. Podoltsev, M. S. Rubin, J. A. Figueroa, M. Y. Lee, J. Kwon, E. Rowen, J. Yu, and R. O. Kerr, Cancer Invest. **28**, 186 (2010).
4. C. M. Schmidt, P. B. White, J. A. Waters, C. T. Yiannoutsos, O. W. Cummings, M. Baker, T. J. Howard, N. J. Zyromski, A. Nakeeb, J. M. DeWitt, F. M. Akisik, S. Sherman, H. A. Pitt, and K. D. Lillemoe, Ann. Surg. **246**, 644 (2007).
5. S. Hirono, M. Tani, M. Kawai, K. Okada, M. Miyazawa, A. Shimizu, Y. Kitahata, and H. Yamaue, Ann. Surg. **255**, 517 (2012).
6. S. Kawamoto, L. P. Lawler, K. M. Horton, J. Eng, R. H. Hruban, and E. K. Fishman, AJR Am. J. Roentgenol. **186**, 687 (2006).
7. O. Nakahara, H. Takamori, M. Iwatsuki, Y. Baba, Y. Sakamoto, H. Tanaka, A. Chikamoto, K. Horino, T. Beppu, K. Kanemitsu, Y. Honda, K. Iyama, and H. Baba, Ann. Surg. Oncol. **19**, S565 (2012).
8. K. W. Kim, S. H. Park, J. Pyo, S. H. Yoon, J. H. Byun, M. G. Lee, K. M. Krajewski, and N. H. Ramaiya, "Imaging features to distinguish malignant and benign branch-duct type intraductal papillary mucinous neoplasms of the pancreas: a meta-analysis," Ann. Surg. (to be published).
9. M. Chandra, J. Scheiman, D. Heidt, D. Simeone, B. McKenna, and M. A. Mycek, J. Biomed. Opt. **12**, 060501 (2007).
10. Y. Liu, R. E. Brand, V. Turzhitsky, Y. L. Kim, H. K. Roy, N. Hasabou, C. Sturgis, D. Shah, C. Hall, and V. Backman, Clin. Cancer Res. **13**, 4392 (2007).
11. N. Iftimia, S. Cizginer, V. Deshpande, M. Pitman, S. Tatli, N. A. Iftimia, D. X. Hammer, M. Mujat, T. Ustun, R. D. Ferguson, and W. R. Brugge, Biomed. Opt. Express **2**, 2372 (2011).
12. D. B. Evans, G. R. Varadhachary, C. H. Crane, C. C. Sun, J. E. Lee, P. W. Pisters, J. N. Vauthey, H. Wang, K. R. Cleary, G. A. Staerkel, C. Charnsangavej, E. A. Lano, L. Ho, R. Lenzi, J. L. Abbruzzese, and R. A. Wolff, J. Clin. Oncol. **26**, 3496 (2008).
13. J. S. Leeds, M. N. Nayar, M. Dawwas, J. Scott, K. Anderson, B. Haugk, and K. W. Oppong, Pancreatology **13**, 263 (2013).
14. R. H. Wilson, M. Chandra, J. Scheiman, D. Simeone, B. McKenna, J. Purdy, and M. A. Mycek, Opt. Express **17**, 17502 (2009).
15. H. Dehghani, M. E. Eames, P. K. Yalavarthy, S. C. Davis, S. Srinivasan, C. M. Carpenter, B. W. Pogue, and K. D. Paulsen, Commun. Numer. Methods Eng. **25**, 711 (2009).
16. M. Jermyn, B. W. Pogue, H. Ghadyani, S. C. Davis, M. Mastanduno, and H. Dehghani, in *Biomedical Optics*, OSA Technical Digest (Optical Society of America, 2012), paper BW1A.7.